International Journal on Interactive Design and Manufacturing (IJIDeM)
https://doi.org/10.1007/s12008-024-01814-1

ORIGINAL ARTICLE

Accelerating the design of gerotor pumps using interactive tools and fast simulation

Juan Pareja-Corcho[1,4] · Asier Pedrera-Busselo[2] · John Ciarrusta[2] · Aitor Moreno[1] · Jorge Posada[1] · Oscar Ruiz-Salguero[1,3]

Received: 21 December 2023 / Accepted: 4 April 2024

Abstract

Gerotors are a family of mechanical pumps used for cooling, lubrication and fuel transfer in aerospace, medicine, etc. Modern industry demands to shorten the development time of products. This means further integration between the different design stages. As in any hydraulic machinery, an important bottleneck in the design process is the simulation time to validate designs. This is due mainly to the fact that Computational Fluid Dynamics (CFD) remains the go-to tool to perform simulations of hydraulic phenomena. One way to reduce this bottleneck is to adopt approximate yet fast simulation routines to refine the design before entering a precise simulation stage. This manuscript presents an interactive design tool that estimates the efficiency response of gerotor pumps using fast simulation routines. The presented tool intends to shorten and accelerate the design cycles of Gerotor pumps by providing the engineer with an estimation of the effect of geometry changes in the pump's efficiencies in real time. The software tool integrates 2D and 3D design capabilities with real-time simulation response. The resulting efficiency estimations differ from the CFD models in maximum 8% in the case of volumetric efficiency. For mechanical efficiency the error ranges between around 20% and 45%, but the pump's internal forces is estimated within a 1% accuracy. Future work focuses on refining the accuracy of the efficiency estimations and further integration of the design tool with physical data.

Keywords Gerotor pumps · Interactive design · Fast simulation · Volumetric efficiency · Mechanical efficiency

List of symbols

$\mathbf{Z}$	Number of teeth in the external gear
$\mathbf{R_2}$	Distance to the center of the generator circumference
$\mathbf{e}$	Eccentricity, distance between the centers of rotation of internal and external gears
$\mathbf{r_2}$	Radius of rolling roulette
$\mathbf{r_1}$	Radius of fixed roulette
$\mathbf{Q_{th}}$	Theoretical flowrate of the pump
$\mathbf{Q_r}$	Real flowrate of the pump
$\mathbf{V_i}(\theta)$	Volume of chamber i for angular position θ
$\mathbf{P_{in}}$	Pressure at the inlet
$\mathbf{P_{out}}$	Pressure at the outlet
$\mathbf{Q_{ip}}$	Inter-profile leakage
$\mathbf{Q_{vc}}$	Flow through the vena contracta
$\mathbf{j_p}$	Gap between the profiles at contact points
$\mathbf{H_p}$	Area reduction due to energy losses at vena contracta
$\mathbf{b}$	Width of the axial cover flow
$\mathbf{l}$	Length of the axial cover flow
$\mathbf{j_c}$	Axial gap between the rotors and the pump's cover
μ	Viscosity of the fluid
$\eta_{\mathbf{vol}}$	Volumetric efficiency of the pump
$\mathbf{W_{hyd}}$	Power transmitted to the fluid
$\mathbf{W_{vt}}$	Power loss due to viscous effects
$\mathbf{M_v}$	Viscous torque
$\mathbf{F_v}$	Viscous force
$\omega_{\mathbf{int}}$	Angular speed of internal gear

✉ Juan Pareja-Corcho
jcpareja@vicomtech.org

1 Industry and Advanced Manufacturing, Vicomtech Foundation, Mikeletegi 57, 20850 Donostia, Gipuzkoa, Spain

2 Egile Innovative Solutions, Kurutz-Gain Pol. 12, 20850 Mendaro, Gipuzkoa, Spain

3 Laboratory of CAD CAM CAE, Universidad EAFIT, Kr. 49 Cl. 7S 50, Medellin 050022, Antioquia, Colombia

4 Faculty of Informatics, University of the Basque Country (UPV/EHU), Manuel Lardizabal 1, 20018 Donostia-San Sebastian, Gipuzkoa, Spain

Published online: 24 April 2024

$\mathbf{r_{er}}$	Radius of the equivalent ring simplification
$\mathbf{W_p}$	Power loss due to pressure effects
$\mathbf{M_p}$	Viscous torque
$\mathbf{F_i}$	Pressure force applied by the fluid to the walls of volume chamber i
$\mathbf{r_i}$	Vector from center of rotation to virtual point where force F_i is applied
$\eta_{\mathbf{mec}}$	Mechanical efficiency of the pump

1 Introduction

Gerotor pumps [1] are internal gear pumps widely used in aerospace [2], automotive [3], manufacturing [4] and other applications. Gerotors are a popular choice for low pressure applications because of their simplicity, compactness and reliability [4].

A gerotor pump consists of two gears (also called *rotors*) (Fig. 1). The external gear features n teeth and the internal gear features $n-1$ teeth. Both gears rotate around their respective axes with constant angular speed. The center of rotation of the external gear is displaced a distance e (known as eccentricity) with respect to the center of rotation of the internal gear. The angular velocities of the internal and external gears are related by the number of teeth in both gears ($\omega_{\text{ext}} = \frac{n-1}{n}\omega_{\text{int}}$). The cavities (volume chambers) between the internal and external rotor are filled with fluid, which is displaced by the variation of the volume chambers. The charge and discharge of the fluid occurs through *port* structures that connect the hydraulic system to the volume chambers in the pump (shown in Fig. 1b).

The shape of the curve describing the internal gear determines the performance of the pump. This performance is measured in many ways according to the context of operation, but two main quantities are commonly used to measure the energy efficiency of the pump [5]: the volumetric efficiency, which refers to the amount of fluid the pump actually delivers in relation to what it could deliver under ideal conditions; and the mechanical efficiency, which refers to the amount of energy transmitted to the fluid in relation to the amount of energy used to run the pump. When designing a pump the engineer seeks to maximize these two quantities.

1.1 Interactive design and fast simulation

In the context of Product Lifecycle Management (PLM), new trends point towards reducing the product development time [6]. For industrial components, this poses the challenge of further integration between the different design stages, specially between what Beitz et al. [7] call the *embodiment* design stage (i.e. where the product architecture is shaping up) and the *detail* design stage, where the final product specifications are defined and validated with respect to the product

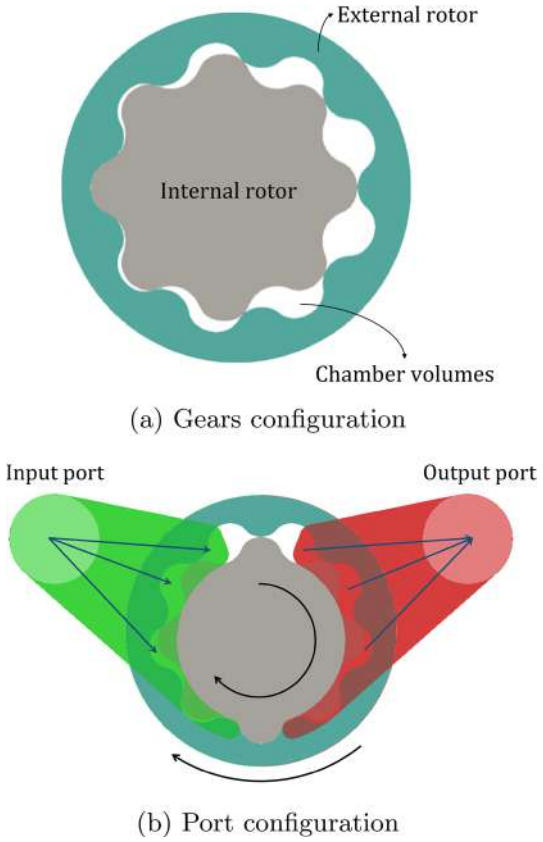

Fig. 1 General architecture of a gerotor pump. Blue arrows depict the direction of the fluid flow (Color figure online)

requirements. This amounts, in other words, to accelerate the convergence of the design space towards the final product specification by speeding the loop between the design variations and expected outcome.

In the case of Gerotor pumps, the design is driven by (a) hard constraints from the particular application (size, noise, flowrate, etc.) and (b) softer and more general constraints such as efficiency, ecological footprint, cost and reliability. A good design must comply with the hard constraints while at the same time optimizing the softer constraints. How a design fares with respect to these constraints is measured by simulation. However, the simulation of hydraulic phenomena requires the use of time- and computation-intensive methods such as Computational Fluid Dynamics (CFD). This is where fast albeit approximate simulation methods are needed to enable the interactive design of pumps. Fast simulation methods integrated in design tools produce better designs that can then be tested with intensive detailed methodologies.

In this paper a software tool is introduced that integrates geometric design and fast estimation of the pump's performance (flowrate, volumetric efficiency and mechanical efficiency) to aid the engineer in the decision making process with the goal of reducing the pump's development time (Fig. 2).

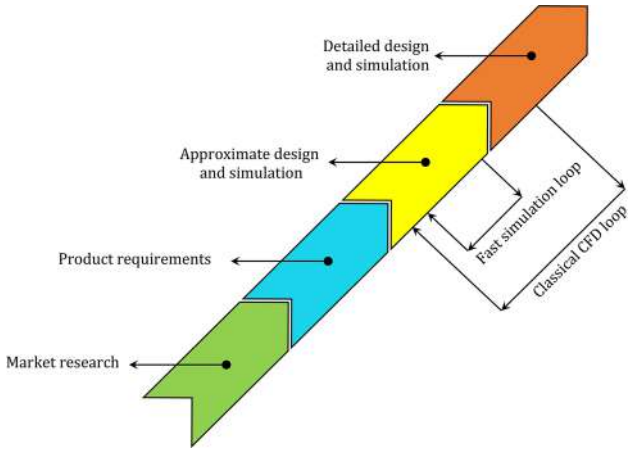

Fig. 2 The fast simulation place in the design process

2 Related works

The methods used to study the behaviour of Gerotors can be classified in two families: (a) CFD-based models and (b) analytical models. Many authors study the relation between the Gerotor profile and its delivered flowrate, pressure ripple and contact forces by using commercial CFD tools [5, 8–10]. These studies can capture precisely the geometry of the pump and simulate its performance under a wide range of operation conditions. This approach, however precise it might be, requires an enormous amount of computing time. Castilla et al. [10] remark that most studies addressing the Gerotor performance are numerical studies corroborated by experimental work on already manufactured pumps and few works relate to the early design stages. This supports the claim that CFD models are suitable only for a late design stage, where specific details should be captured and precision is needed, but are not well suited to be used in contexts where interactiveness and real-time response is needed.

Some analytical approaches exist in the literature. Lee et al. [11] address the calculation of the theoretical displacement as the difference between the maximum and the minimum chamber areas in a particular angular position of the pump. Ivanovic et al. [12] calculate the theoretical displacement as the integral of the change in volume over an angular differential. Both methods are able to capture the flowrate pulsation of the pump and exhibit similar errors with respect to experimental data, but do not address the calculation of the actual flowrate of the pump. Gamez-Montero and Codina [13] present a mathematical model to estimate the actual flowrate of a trochoidal gerotor pump considering variable height clearances between profiles. Lingeswaramurthy et al. [14] estimate the actual flowrate using the pressure build-up equation. This approach does not consider the effect of geometric clearances. Liu et al. [15] estimates the actual flowrate by calculating the change ratio of area between inner and outer rotors in the outlet region. This approach does not consider the leakages produced by geometric clearances. Harrison et al. [16] presents a model that estimates the actual flowrate using constant clearance height between profiles but does not consider inter-faces leakages.

The estimation of the mechanical efficiency of gerotor pumps entails the approximation of the power lost by the action of internal forces. In the reviewed literature, these forces are of three types: (i) viscous friction forces, (ii) contact forces between gears and (iii) fluid pressure forces. Harrison et al. [16] present an analytical friction model to estimate the power consumption of a gerotor pump. This friction-only model shows good correlation with experimental data but fails to consider other sources of power loss. Inaguma [17] present a mathematical model to estimate the friction torque in any internal gear pump. That model is used by the same Inaguma [18] to predict power loss at different operation temperatures. The main drawback of Inaguma's method is that it uses a set of pump constants that must be calculated by experimental results. This forbids its use in an early design stage.

Contact forces between gears and the stresses they induce are mostly studied with the use of CFD/FEA tools. Ivanovic [19] and Kwak et al. [20] study the effect of geometrical parameters on the contact forces and power loss using finite element analysis. Ivanovic et al. [21] present an analytical model to estimate the contact loads in trochoidal gerotor pumps which underestimates the contact stresses with respect to FEA calculations. This methodology does not address the influence of contact stresses on power loss. Ivanovic et al. [22] present models for both contact forces and fluid pressure forces and their effect on the power loss. The fluid pressure model is based on the numerical solution of the equilibrium equations for every angular position. The calculations required for this methodology are not suitable for real-time interactiveness, yet faster than CFD/FEA methods. Some machine learning approaches exist in the general field of centrifugal pumps [23] and other methodologies from different fields [24] could be adapted to the case of Gerotor pumps. The main drawback of these approaches is the need for data from manufactured pumps with a wide range of designs and operating conditions to account for the variability of the prediction. It is expected that new developments in pump design arise in the field of Machine Learning and Artificial Intelligence.

As for the use of interactive design tools in the Gerotor design and validation, to our knowledge very few studies address the integration of existing or new analytical methods in comprehensive design software tools. Gamez-Montero et al. [25] present an early tool called *GeroLAB* which integrates 2D design, volumetric flowrate and contact stress calculations. As the concept of Digital Twin gains popularity in industry [26], it is expected that new tools for real-time

interaction between virtual prototypes and physical pumps become important in the following years. A review of the use of Digital Twins in the field of fluid machinery [27] found that most applications are limited to the monitoring of the operation of real equipment.

To partially overcome the mentioned shortcomings, this manuscript presents the implementation of an interactive design tool to aid the engineer in the decision-making process. To achieve this, 2D and 3D design, fast estimation of performance indexes and data visualization are integrated in a single software tool. Additionally, the models used to estimate the performance indexes are explained. The **volumetric efficiency** is estimated using constant clearances and considering the combined effect of inter-profile and inter-face leakages. The **mechanical efficiency** is estimated considering the combined effect of a viscous force model and a fluid pressure model. The models presented are analytical simplifications of numerical models that avoid time expensive calculations and thus to allow near real-time interaction.

$$\begin{aligned} P'_x(\theta) &= \cos(Z\,\theta)\left(e - \frac{S\,r_2}{m}\right) \\ &\quad - R_2\,\cos(\theta)\left(\frac{S}{m} - 1\right) \end{aligned} \tag{1}$$

$$\begin{aligned} P'_y(\theta) &= R_2\,\sin(\theta)\left(\frac{S}{m} - 1\right) \\ &\quad - \sin(Z\,\theta)\left(e - \frac{S\,r_2}{m}\right) \end{aligned}$$

$$m = \sqrt{{R_2}^2 + 2\,\cos(\theta\ (Z-1))\ R_2\,r_2 + {r_2}^2} \tag{2}$$

3 Methodology

In this section, the Gerotor's geometry is discussed, the performance models are explained and validated and the software tool is introduced.

3.1 Geometric modeling of a gerotor pump

Gerotor pumps can be classified according to the nature of the curve describing its internal gear. This paper considers *trochoidal* gears. Morley [28] defines *trochoidal* curves as the locus of a point fixed to a circle that rolls without slipping around a fixed circle. However, pumps designed in this way show very high wear and tightness issues, as stated by Gamez-Montero [29]. To alleviate these issues, a *modified trochoidal* profile is used to design the internal gear. This is built as shown by Fig. 3a.

A circumference of radius r_2 with center at O' rolls without slipping over a fixed circumference of radius r_1 with center at O_1. This movement entails an instantaneous center of rotation I located in the line $O'O_1$. Additionally, a line $O'P$ with fixed length R_2 is created with an angle $\phi = \theta/Z$, where θ is the angle of the rolling movement. This line generates a point P. A circumference with radius S centered at P is drawn. The intersection between this circumference and the line IP is the generator point P'. The trace of this point as the movement develops generates the modified trochoidal profile. The parameterized expression for the internal profile is shown in Eqs. 1 and 2.

The external profile can be computed in two ways: by linked circular arcs or by the conjugate curve. The linked circular arc profile is calculated by considering Z circular arcs of radius S equally distributed over a circumference of radius R_2. The arcs are then linked together by a circumference of radius G, as shown in Fig. 3c. This results in an external gear profile that does not mesh perfectly with the internal profile, but is commonly used because of the simplicity of its construction. Other possibility is to compute the external profile as the envelope of the family of curves produced by the movement of the internal profile. This approach produces an external gear as the one shown in Fig. 3b.

3.2 Volumetric efficiency

The volumetric efficiency η_{vol} is defined as the ratio between the theoretical flowrate Q_{th} and the actual flowrate delivered by the pump Q_r. Consider the chambers in contact with the output port at a given angular position θ_i. For the time the pump reaches position θ_{i+1}, such chambers will have decreased their volume by an amount ΔV. For a given angular position θ_j, the instantaneous theoretical flowrate corresponds to the amount of fluid disallowed by the change of volume of all chambers in contact with the output port:

$$Q_{th}(\theta_j) = \sum_i \frac{\partial V_i}{\partial \theta}(\theta_j) \tag{3}$$

In Eq. 3, index i corresponds to the index of all chambers in contact with the output port at any given angular position. Notice that this definition assumes that the chambers in contact with the output port discharge **all** the fluid that corresponds to the decrease in volume ΔV. It is well known that this assumption is not true in the real operation of the pump because of (i) fluid leakages (addressed in this methodology) and (ii) partial discharges (not addressed in this methodology). In the present methodology two sources of fluid loss are considered: (a) inter-profiles leakage $\left(Q_{ip}\right)$ and (b) inter-faces leakage $\left(Q_{if}\right)$. Inter-profiles leakages occur because of the imperfect sealing between adjacent volume chambers. Inter-faces leakages occur because of the pressure delta in the film of fluid between the faces of the rotors and the surrounding cover. The real flowrate Q_r of the pump is obtained

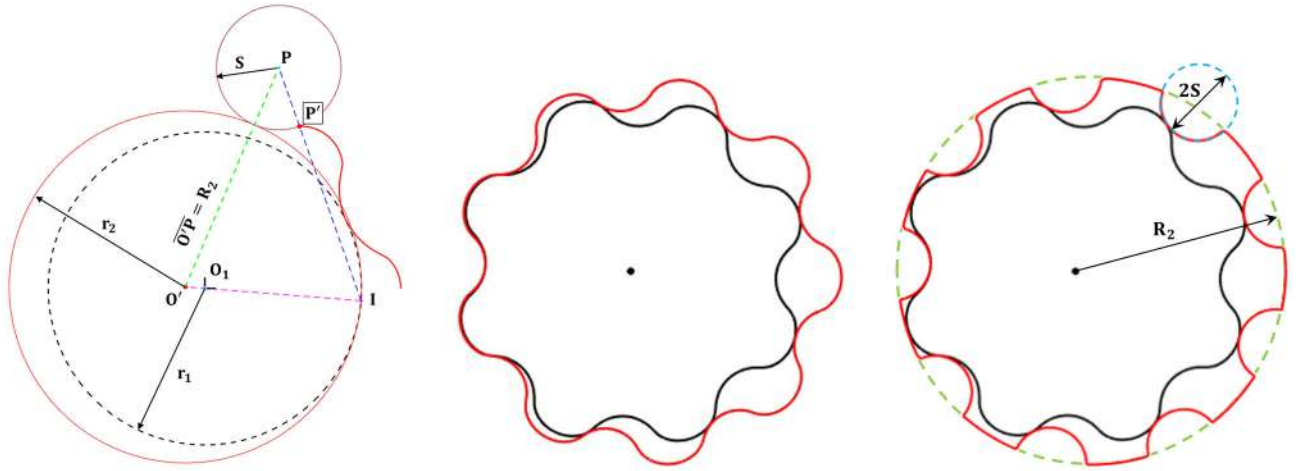

(a) Modified trochoidal profile generation (b) Pump with conjugated external profile (c) Pump with circular arc external profile

Fig. 3 Geometric modeling of a trochoidal Gerotor pump

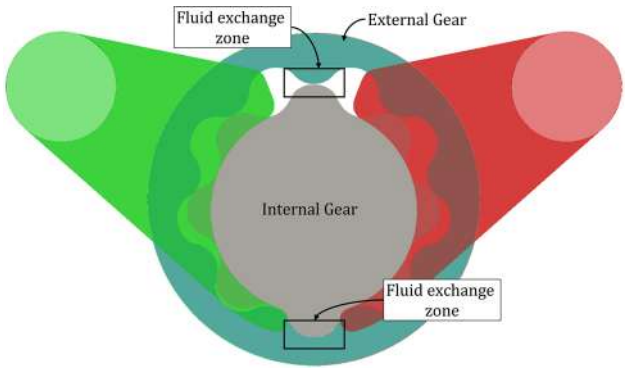

Fig. 4 Inter-profiles leakages in a Gerotor pump

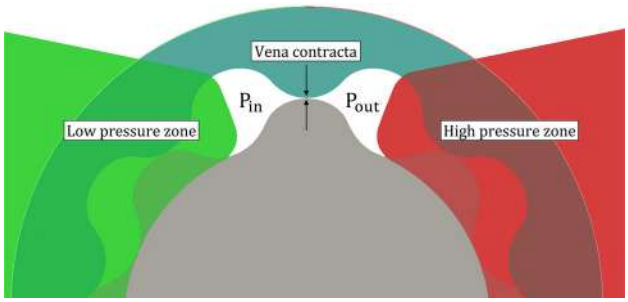

Fig. 5 Pressure differential $\Delta P = P_{out} - P_{in}$ induces a flowrate through the *vena contracta* as $P_{out} > P_{in}$

by substracting the fluid lost in the leakages to the theoretical flowrate.

3.2.1 Inter-profiles leakage

The volume chambers in a Gerotor pump are defined as the empty pockets between the internal and external gears. Ideally, two adjacent volume chambers should be isolated from each other at all times to prevent fluid exchange between them. It is known that in practice this is not possible given that: (i) manufacturing techniques cannot consistently produce perfectly meshing gears, and (ii) even when there is perfect meshing, it is not completely desirable as it increases the contact stresses in the gears. As a result of this, a geometric clearance j_p appears between adjacent volume chambers (Fig. 4). This geometric clearance entails the possibility of the exchange of working fluid between adjacent volume chambers.

The exchange of fluid between adjacent chambers through the gap between profiles occurs when the adjacent chambers have a different instantaneous pressure. The difference in pressure induces an exchange of fluid. At any angular position of the pump, each chamber is subjected either to the pressure of the input port P_{in} or the pressure of the output port P_{out}. Therefore, the exchange of fluid due to the inter-profile gap only happens in the pairs of volume chambers where the transition between the ports is made (Fig. 5).

The inter-profile gap is the point where the cross-sectional area of the fluid stream is minimal. It is assumed that the flow in this area behaves as a vena contracta. Therefore, the flowrate Q_{vc} through the inter-profile gap is modeled as shown in Eq. 4 [30]:

$$Q_{vc} = A_{vc}\sqrt{\frac{2\Delta P}{\rho}} \rightarrow A_{vc} = H(j_p - H_p) \tag{4}$$

The area of the vena contracta A_{vc} corresponds to the cross-sectional area through which the fluid exchange takes

place. It is a well known result of fluid mechanics that the area of the fluid jet in a vena contracta is smaller than the area of the orifice through which it flows. This reduction in the area of the fluid accounts for the energy loss in the contraction and is related to the geometry of the orifice. As a result of this, the area of the vena contracta A_{vc} is calculated considering the height of the gap j_p (assumed as constant throughout the operation of the pump), a reduction height H_p due to the local geometry of the vena contracta and the width H of the rotors. The described fluid exchange takes place in the superior and inferior sides of the pump. Notice that the output pressure P_{out} is always larger than the input pressure P_{in}. Therefore, the fluid flow through the inter-profile gap always moves in the direction of the input port and away from the output port. This entails that the fluid exchange thorugh the inter-profile gap is in fact a leakage. The inter-profile leakage is twice the flow through the vena contracta $\left(Q_{if} = 2\ Q_{vc}\right)$ as this flow exchange happens in two different places in the pump.

Notice that the vena contracta formulation does not consider the viscosity of the fluid (i.e. considers the fluid as a "perfect fluid"). A more comprehensive model should be proposed to account for the viscosity of the fluid or to determine how much the behaviour of perfect fluid deviates from that of viscous fluid in a vena contracta.

3.2.2 Inter-faces leakage

The inter-faces leakage refers to the fluid exchange between the high and low pressure chambers through the fluid film between the gears faces and the pump's cover. The fluid flows from the high pressure chamber to the low pressure chamber through an area of contact between the two chambers (Fig. 6). This interaction occurs in both the superior and inferior part of the pump and in both superior and inferior sides of the gears (Eq. 5).

$$Q_{if} = Q_{1,sup} + Q_{1,inf} + Q_{2,sup} + Q_{2,inf} \tag{5}$$

The total flowrate for the inter-faces leakage is the sum of the four independent flowrates on both sides of the gears and the superior and inferior part of the pump. The model considers each flowrate as a flow between two stationary plates subjected to a pressure differential (Fig. 6) [30]. This is known as the Poiseuille flow model and assumes the flow in this region is laminar (Eqs. 7 and 7).

$$Q_{1,sup} = Q_{2,sup} = \frac{b_{sup}\ j_c^3\ \Delta P}{12\ \mu\ l_{sup}} \tag{6}$$

$$Q_{1,inf} = Q_{2,inf} = \frac{b_{inf}\ j_c^3\ \Delta P}{12\ \mu\ l_{inf}} \tag{7}$$

Distances l_{sup} and l_{inf} are calculated as the minimum distance between the input and output ports in their respective halves (superior and inferior) of the pump. Distances b_{sup} and b_{inf} are calculated as the vertical distance from the shaft bore to the outermost circumference of the external gear. Interface clearance j_c does not necessarily coincide with the port width as alternative designs can be conceived where these two distances are not the same.

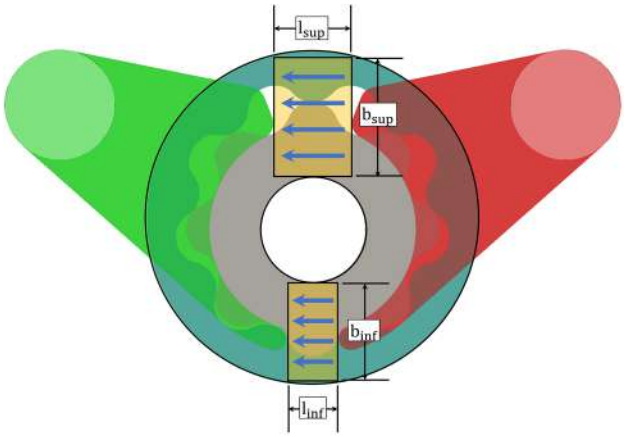

(a) Top view of the interface leakage zone

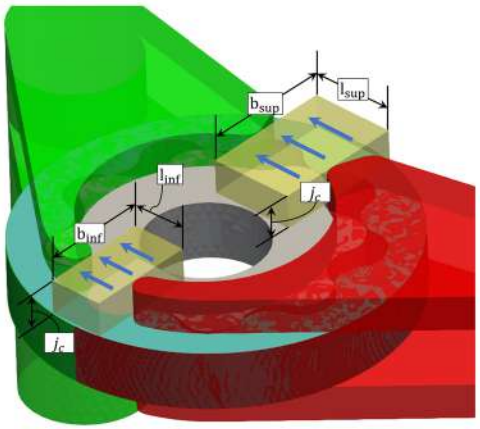

(b) Isometric view of the interface leakage zone

Fig. 6 Inter-faces leakages in the gerotor pump

3.3 Mechanical efficiency

The mechanical efficiency refers to the ratio between the power transfered to the fluid W_{hyd} (also called hydraulic power) and the total power drained from the driving engine $W_{hyd} + W_{loss}$. The hydraulic power is calculated using the real flowrate and the pressure differential applied to the fluid, as in Eq. 8.

$$W_{hyd}(\theta) = Q_r(\theta)\ \Delta P \tag{8}$$

The power loss W_{loss} must be calculated by considering the internal forces that appear in the operation of the pump. These internal forces entail resisting torques with respect to the center of rotation of both gears. The resisting torques represent power *leakages* (with respect to a particular angular velocity) that use some of the power drained from the engine to counter the action of those forces. In this paper two sources of resisting torques are considered: (a) viscous torque and (b) chamber pressure torque. The total power loss is calculated as the sum of the effect of the power lost due to the viscous torque and the power lost due to the pressure torque.

3.3.1 Viscous power loss

The viscous torque is the torque induced by the action of the viscous forces that appear in the moving gears faces. During the operation of the pump, these gears faces are in contact with a film of fluid that *resists* the movement of the gears. The power loss due to the effect of the viscous torques is calculated as shown in Eq. 9.

$$W_{vt} = M_{v,int}\ \omega_{int} + M_{v,ext}\ \omega_{ext} \tag{9}$$

$M_{v,int}$ and $M_{v,ext}$ are the viscous torques on the internal and external gears, respectively. To simplify and accelerate the calculation of the viscous torques, a geometrical simplification of the gears is considered. This simplification is known as the *equivalent ring* of the gear (Fig. 7). The *equivalent ring* of a gear with area A_g and a fixed internal radio of r_f is the ring with internal radio of r_{er} and area $A_g/2$. Radio r_{er} is the radio that splits the area of the gear in half. Figure 7 shows the calculation of the equivalent rings for the internal and external gears. In the case of the internal gear, the internal radio is fixed and external radio r_{er} is found. In the case of the external gear, the external radio is fixed and the internal radio r_{er} is found.

The viscous torque in each gear is calculated as the torque produced by the action of the viscous force F_v (that, by definition, always opposes the direction of the movement) over the equivalent ring radio (r_{er}) of each gear with respect to their individual centers of rotation (Fig. 8, Eqs. 11 and 11):

$$M_{v,int} = F_{v,int}\ r_{er,int} \tag{10}$$

$$M_{v,ext} = F_{v,ext}\ r_{er,ext} \tag{11}$$

Consider the case of fluid between a surface moving with constant velocity V and a stationary surface separated by a distance h. The viscous force F_v at the moving surface is the sum of the tangent shear stresses throughout the entire area of that surface. This translates to a formulation of the viscous force in terms of the area of the surface A, the viscosity of the fluid μ and the velocity gradient of the fluid (Eq. 12).

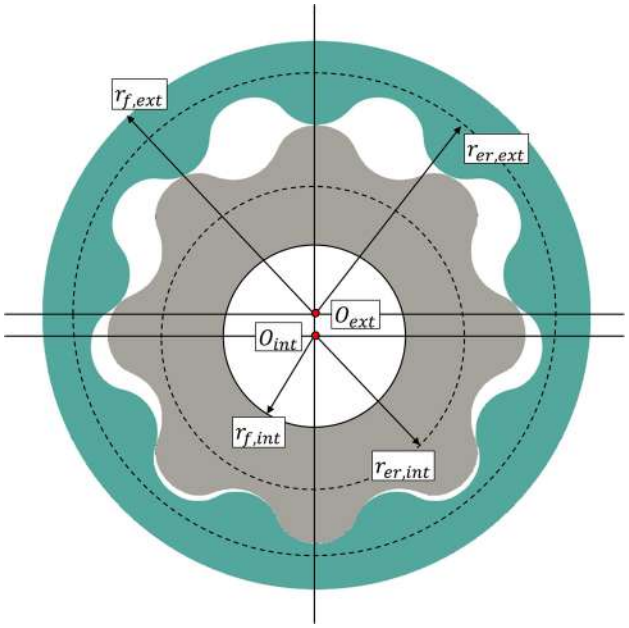

Fig. 7 Equivalent ring radii for the external $r_{er,ext}$ and internal $r_{er,int}$ gears

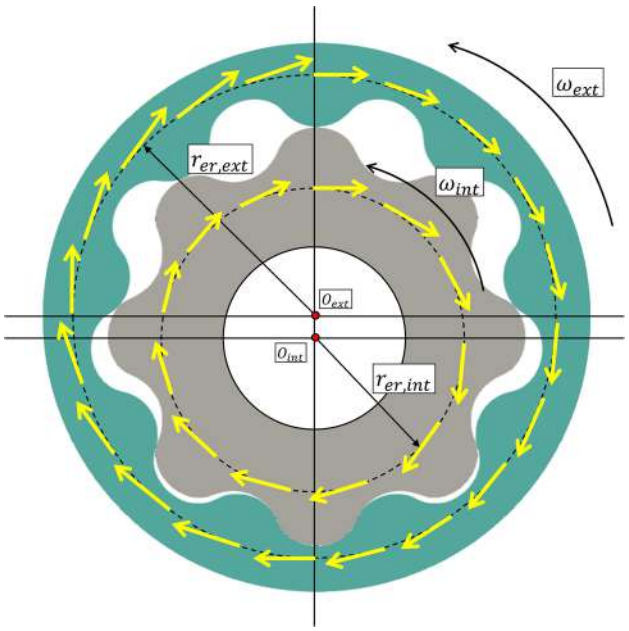

Fig. 8 Viscous force distribution over the equivalent rings

$$F_v = \int \tau_{xz(y=0)}\ dA = A\ \mu\ \frac{dv}{dy}_{(y=0)} \tag{12}$$

Solving the Navier–Stokes equation for the conditions of a stationary surface and no-slip at the moving surface, an expression for the velocity gradient between the surfaces can

be obtained:

$$\frac{dv}{dy} = \frac{1}{2\mu}\frac{dp}{dx}(2y - h) - \frac{V}{h} \tag{13}$$

where $\frac{dp}{dx}$ is the pressure gradient in the x direction. In the case of the present model, the pressure gradient $\frac{dp}{dx} = \Delta P$ is the difference between the pressures at the input and output ports and the distance h corresponds to the distance j_c between the faces of the gears and the outer cover. The linear velocity V of the moving surface (which corresponds to the face of the gear) is found as $\mathrm{V} = \omega\, r_{er}$. Equation 13 can be rewritten in terms of the parameters of the gerotor pump as:

$$\frac{dv}{dy} = \frac{1}{2\mu}\Delta P\,(2y - j_c) - \frac{\omega\, r_{er}}{j_c} \tag{14}$$

By evaluating Eq. 14 at $y = 0$ and using the adequate angular velocity ω (depending on the gear being calculated), it is possible to find the values for the viscous forces on both gears ($F_{v,int}$ and $F_{v,ext}$). With the known viscous forces, the power loss W_{vt} due to the viscous torque can be calculated. The proposed methodology assumes the flow between the faces of the gears and its cover is of laminar nature. This assumption is sensible since viscous fluids are more likely to present laminar behaviour for low Reynolds numbers.

3.3.2 Pressure power loss

The pressurized fluid in the chambers applies pressure on the walls of the gears that enclose each volume chamber. To accelerate the calculation of the pressure-induced torque, the following is assumed: (a) every point inside an individual chamber has the same pressure at a given angular position and (b) each individual chamber applies the same pressure to the internal and external gear walls. It is known from more detailed simulations that this is not strictly true but considering otherwise would mean an undesired volume chamber discretization and costly numerical method. The pressure-induced power loss is calculated as shown in Eq. 15.

$$W_{pt}(\theta) = M_{p,int}(\theta)\,\omega_{int} + M_{p,ext}(\theta)\,\omega_{ext} \tag{15}$$

$M_{p,int}(\theta)$ and $M_{p,ext}(\theta)$ are the pressure-induced torques in the internal and external gears, respectively. The procedure to calculate the pressure-induced torques for both gears is the same. Only the procedure to calculate the pressure-induced torque for the internal gear $M_{p,int}$ is detailed. The pressure-induced torque on the internal gear is calculated as the combined effect of the torques produced by all n volume chambers in the pump. The torque of each individual chamber is calculated as the vectorial product of a position vector and a force vector:

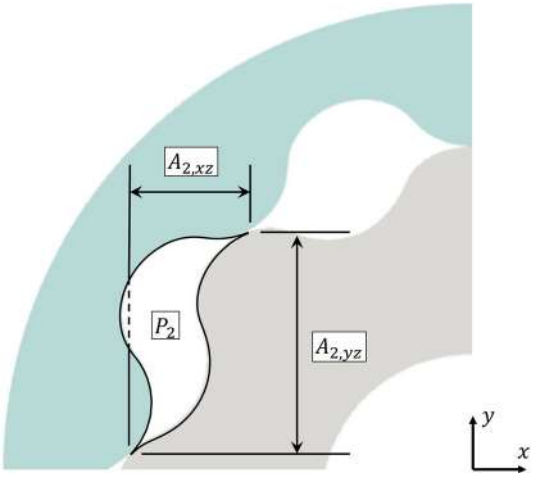

Fig. 9 Calculation of equivalent force $\mathbf{F}_{i,int}$ as pressure over a projected area

$$M_{p,int}(\theta) = \sum_{i=0}^{n} M_{i,int}(\theta) = \sum_{i=0}^{n} \mathbf{r}_{i,int}(\theta) \times \mathbf{F}_{i,int}(\theta) \tag{16}$$

In Eq. 16, the term $\mathbf{F}_{i,int}$ is the equivalent force that the pressure P_i in chamber i applies to the walls of the internal gear. The term $\mathbf{r}_{i,int}$ is the position vector of the point of application of the equivalent force with respect to the center of rotation of the internal gear. The equivalent force $\mathbf{F}_{i,int}$ (Eq. 17) is found by distributing the pressure P_i over the projected area of each chamber in the planes A_{xz} and A_{yz}, as depicted in Fig. 9:

$$\mathbf{F}_{i,int} = P_i\; A_{i,yz}\,\mathbf{i} + P_i\; A_{i,xz}\,\mathbf{j} \tag{17}$$

The calculated force for each chamber must be applied somewhere to produce a torque with respect to the rotation center of the gear. The position vector $\mathbf{r}_{i,int}$ of the point of application of the force in each chamber can be written as in Eq. 18.

$$\mathbf{r}_{i,int} = r_{x,i}\,\mathbf{i} + r_{y,i}\,\mathbf{j} \tag{18}$$

The components r_x and r_y are defined as the distance (in each axis) from the center of rotation of the gear (in this case the internal gear) to the medium point of the projected areas $A_{i,yz}$ and $A_{i,xz}$, respectively (Fig. 10).

3.4 The interactive design tool

The models presented need to be integrated in a software tool that makes them usable and accessible for design engineers. The goal of the present tool is to perform all calculations automatically from a set of geometrical and operational

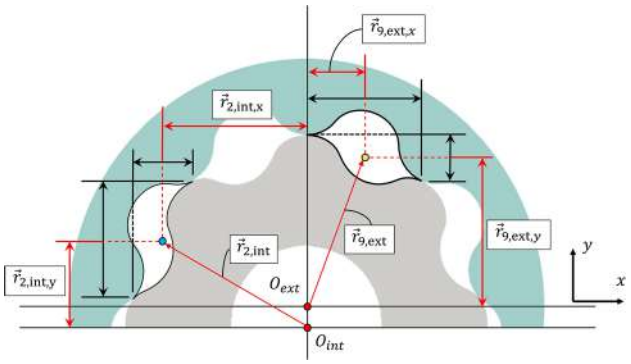

Fig. 10 Calculation of the position vector $\mathbf{r}_{i,int}$ for chamber i

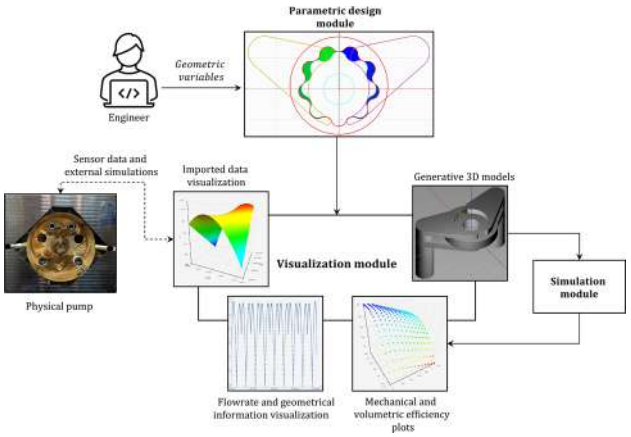

Fig. 11 Architecture of the design tool

parameters. The architecture of this tool is presented in Fig. 11. The tool consists of three modules: the parametric design module, the 3D module and the simulation module. The parametric design module automatically generates the 2-dimensional geometry of a gerotor pump from a set of parametric values provided by the design engineer. The geometry generated includes: (a) the internal trochoidal profile, (b) the external conjugate or circular arc profile, (c) the polylines of the individual volume chambers for any position of the pump, (d) the inlet and outlet ports geometry that fits the desired configuration of the pump. After the geometry of the pump is generated, the history of volumes is calculated for each volume chamber throughout a full revolution of the pump. Additionally, the intersection area between the volume chambers and the inlet/outlet ports are calculated for every angular position of the pump. This information will be used by the simulation module to estimate the pump's efficiency.

The visualization module starts by constructing the 3D CAD models of the 2D geometry defined in the previous step. This construction is done using OpenCASCADE technology and the resulting models are visualized using a Qt + OpenGL framework tailored for fast visualization and animation. The visualization environment provides an animated scene of the pump's gears rotation. The same graphic environment displays: (a) the history of geometric data calculated by the parametric design module, (b) the efficiency data calculated by the simulation module and (c) the data captured from the physical pump and from external CFD simulations.

The simulation module uses the geometrical information generated by the previous modules and operation settings provided by the engineer to estimate the mechanical and volumetric efficiency of the current pump in real-time using the methods provided in previous sections. Figure 12 shows the graphic environment of the design tool. In Fig. 12 the volumetric and mechanical efficiencies were calculated using the following operation settings: input pressure $P_{in} = 1.2$ bar, output pressure $P_{out} = 6.5$ bar and angular speed $\omega_{int} = 11,250$ rpm.

4 Results

In this section the results obtained by the estimation methods are presented. First, the methods used to produce the validation data are introduced and then a comparison between the presented models and the validation data is shown.

4.1 Validation

In order to validate the calculations performed by the fast models various CFD simulations were set up. The CAD models of the different profiles were obtained from the design tool and imported into Twin Mesh, a software tool specifically designed for meshing the fluid regions between the rotors. The tool generates a mesh for each timestep, which was defined as 1 degree of rotation of the outer profile. The inter-profile gap was divided in 30 elements and the axial gap in 10 elements. Element width is biased towards the edges. The same elements are reshaped for each mesh in order to transfer the results from one timestep to the next. The timesteps cover a full pitch angle of the outer rotor. After every pitch angle the first timestep mesh is taken and initialized with the results from the previous timestep. Figure 13 shows an example of the results obtained by the CFD tool. The CFD simulation was conducted under the following operation conditions: input pressure $P_{in} = 1.2$ bar, output pressure $P_{out} = 6.5$ bar and angular speed $\omega_{int} = 11250$ rpm.

The simulated results were validated using measurements from the testbed shown in Fig. 14. An existing Gerotor was simulated using the proposed CFD methodology and maximum flowrate deviations of 10% are found. This error is in line with what was reported by Altare and Rundo [31]. The testbed consists of a pressurized tank with flow restrictors before and after the pump, which are used to regulate inlet and outlet pressures. Pressure is measured inside the pump

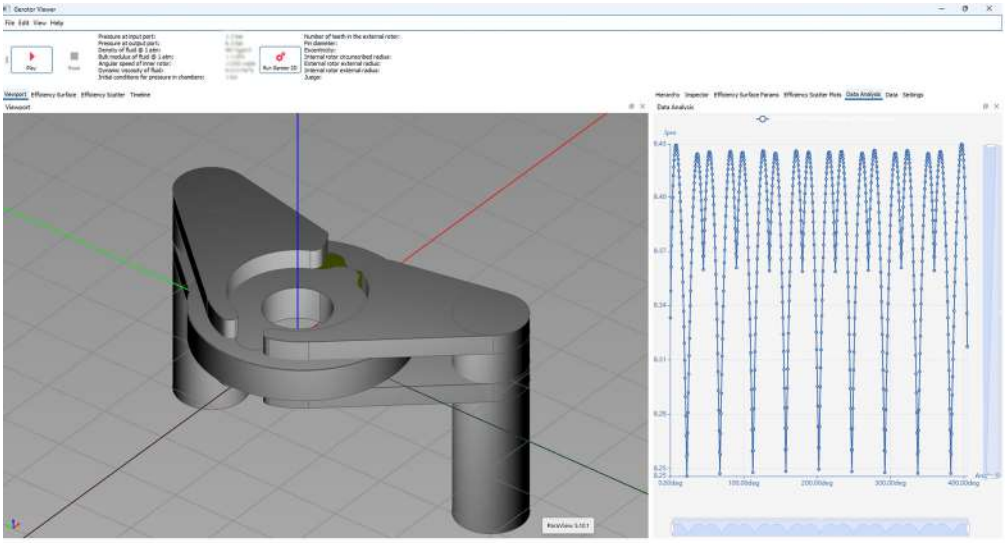

(a) 3D and data visualization mode

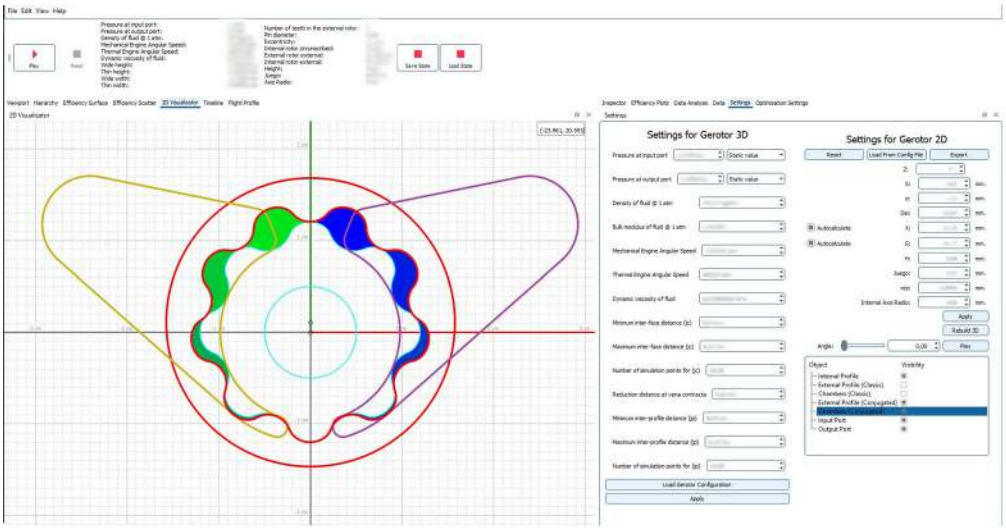

(b) 2D parametric design tool

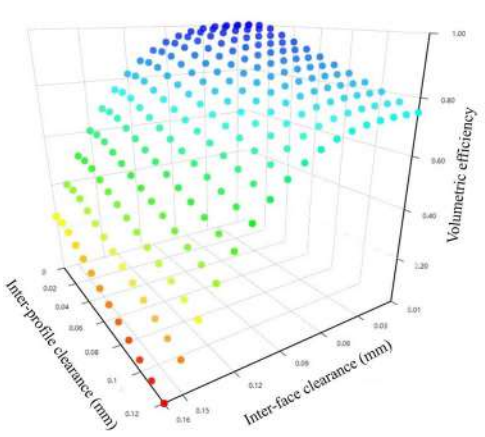

(c) Simulated volumetric efficiency

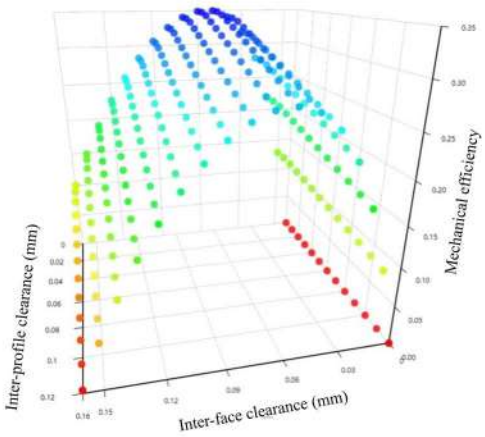

(d) Simulated mechanical efficiency

Fig. 12 Graphic environment of the design tool

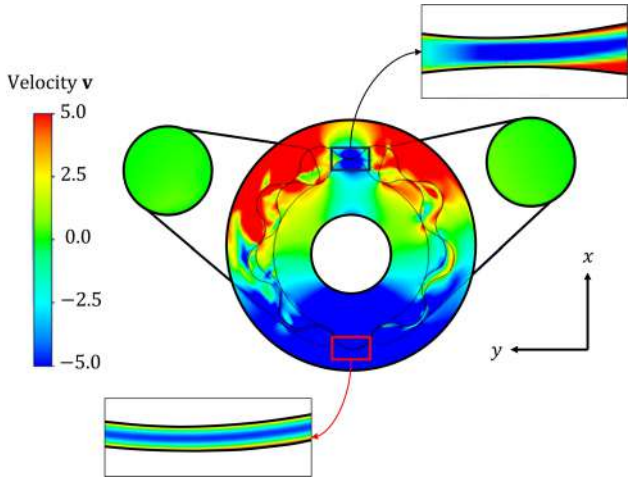

Fig. 13 Fluid flow field in a slice of the Gerotor mesh calculated using CFD simulation

Fig. 14 Dedicated Gerotor testbed

body with STS ATM minisensors. Fluid temperature is measured at various points in the circuit and flowrate is measured right after the pump outlet. The measured value was used to validate the CFD simulations.

In order to validate the methodology to calculate the pressure forces, an FEA simulation was set up. For each volume chamber, the fluid pressure was applied to the surfaces of the internal and external gear. The forces in each chamber and the resultant torque was measured and compared to the resultant pressure torque estimated by the presented method. This process was done for both the maximum volume position and the minimum volume position of the Gerotor (Fig. 15).

4.2 Comparison with presented models

The volumetric efficiency η_{vol} was estimated for several values of the inter-profile clearance j_p and the inter-face clearance j_c. The results are presented in Fig. 16a. The same

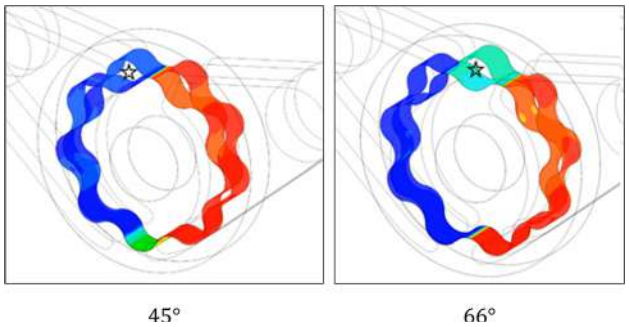

Fig. 15 Pressure application on the walls of the Gerotor

Gerotor profile was simulated using a Computational Fluid Dynamics tool. The results of the CFD simulation are shown in Fig. 16b. The error percentages between presented estimations and the CFD-produced values are presented in Fig. 16c. The maximum error for all the simulated clearances is around 8%. The results show that the calculated error increases as the inter-profile clearance increases. The calculated error does not vary considerably as the inter-face clearance increases.

The reason for the behaviour of the calculated error could be that as the inter-profile clearance j_p increases the *vena contracta* model does not adequately represent the fluid flow between adjacent volume chambers. For smaller values of the inter-profile clearance, the formulation precisely estimates the flow between adjacent volume chambers. The increase of the inter-face clearance j_c does not entail a considerable increase in the calculated error. A possible reason for this is that the accuracy of the model used for this clearance (flow between moving parallel plates) is not affected by an increase in the distance between the plates (represented by the inter-face clearance j_c) as it does not change the basic assumptions of the model. The calculated errors of the volumetric model are compensated by the savings in time and computational expense with respect to the computational fluid dynamics models.

The mechanical efficiency η_{mec} was estimated for the same values of the inter-profile clearance j_p and the inter-face clearance j_c used in the volumetric efficiency estimation. The results are presented in Fig. 16d. The results show that higher values of the inter-profile clearance j_p entail lower mechanical efficiencies. Even though the value of the inter-profile clearance does not influence the mechanical losses, it does influence the actual flowrate of the pump and therefore the hydraulic power. The inter-face clearance j_c influences the value of the viscous resistant torque and therefore the mechanical efficiency of the pump. Results show that small values of the inter-face clearance entail lower mechanical efficiencies. The mechanical efficiency increases as the inter-face clearance increases until the clearance value surpasses a critical level where the mechanical efficiency starts to decrease. The mechanical efficiency was calculated for the

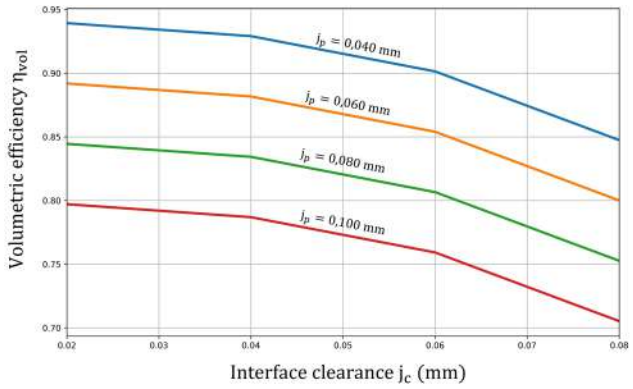

(a) Volumetric efficiency η_{vol} by presented models.

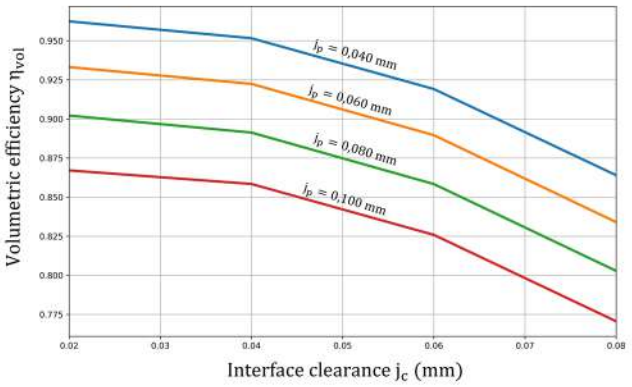

(b) Volumetric efficiency η_{vol} with a CFD tool.

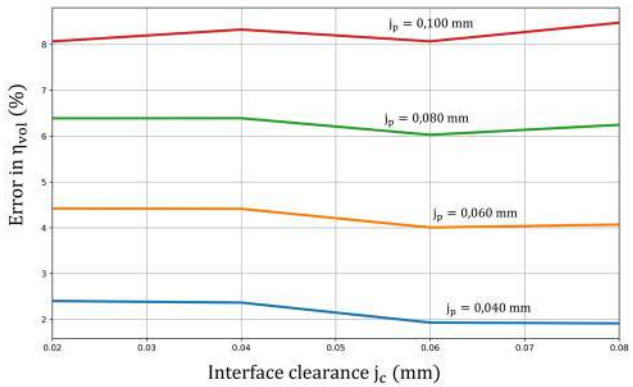

(c) Percentage of error between presented model's estimation and CFD.

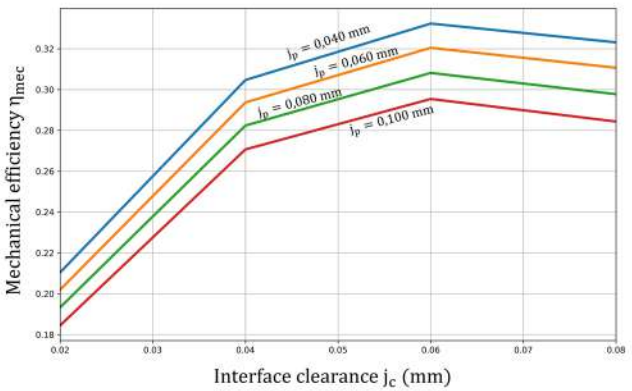

(d) Mechanical efficiency η_{mec} estimated by presented models.

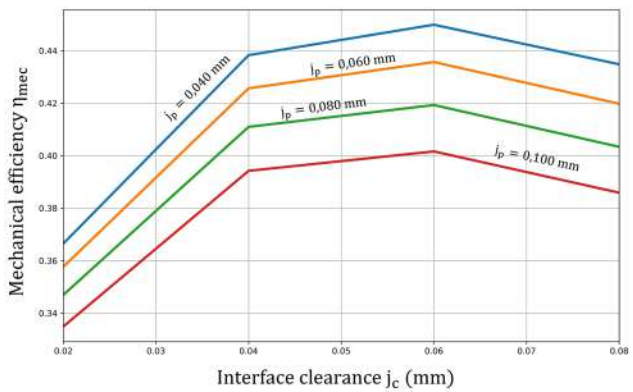

(e) Mechanical efficiency η_{mec} calculated with a CFD tool.

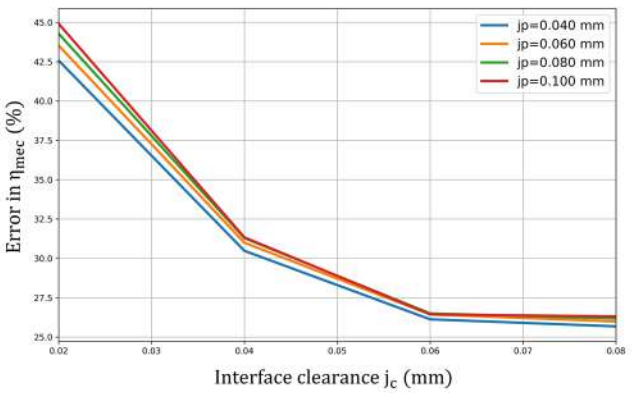

(f) Percentage of error between the between presented model's estimation and CFD.

Fig. 16 Efficiency estimation using fast simulation. Comparison versus CFD models

same profile and the same values of the inter-profile and inter-face clearances using a computational fluid dynamics tool. The results of the CFD simulations are presented in Fig. 16e. The error percentages of the estimations with respect to the CFD models are presented in Fig. 16f.

The calculated errors for the method shows high errors (around 40%) for low values of the inter-face clearance. As the clearance increases, the error with respect to CFD dimishes to around 25%. Lower values of the inter-face clearance increase the effect of the equivalent ring simplification

Table 1 Resultant torques on the pump's rotors as estimated by presented models vs FEA software

Ch	FEA		Present method	
	Internal	External	Internal	External
1	− 0.00	0.00	0.00	0.00
2	− 11.07	− 8.53	10.58	9.04
3	− 14.15	− 15.99	14.34	15.05
4	− 5.71	− 18.54	13.41	10.13
5	− 45.50	44.30	38.07	− 35.42
6	8.39	− 8.21	− 7.02	6.54
7	1.05	3.50	− 2.47	− 1.87
8	2.61	2.90	− 2.64	− 2.77
9	2.04	1.57	− 1.95	− 1.67
Sum	**62.33**	**−0.99**	**62.30**	**−0.97**

All values in Nmm

The numbers that correspond to the Sum of the torques for all chambers (Ch) are in bold

of the rotors of the pump (see Eq. 14). The results show that the model can be improved by developing a more precise way to model the distribution of the viscous forces in the exposed faces of the rotors.

The mechanical model can however estimate very accurately the resultant torque that the fluid exerts on the gears at any time. The resultant torque estimated by the model is validated with respect to a simulation using Finite Element Analysis. Results for the torque generated by these forces are shown in Table 1, for both the internal gear and external gear.

5 Conclusions

Modern industry demands shorter development cycles, more efficient products and faster decision making. To meet these demands, design methodologies trend towards more integration between the different design stages. In the particular case of Gerotor pumps this integration requires tools to aid the engineer to converge faster to the final design of the product that meets the operational requirements. Current design workflows use time- and computation-intensive methodologies even at stages where they might not be needed, thus slowing down the development cycle. A design tool that integrates 2D parametric design, 3D geometry generation, CAD visualization, fast simulation and data visualization in real time is proposed. The fast analytical simulation routines in the design tool can produce results within seconds, contrary to CFD-based established methods, which should be used only in the latter stages of the design workflow. These routines estimate the volumetric and mechanical efficiency of the pump given only a set of geometric parameters and operational conditions. The proposed volumetric model accurately estimates the volumetric efficiency of the pump to maximum errors of 8% with respect to CFD simulations. The mechanical model correctly estimates the internal forces of the gears but results in errors from 25 to 40% in the estimation of the mechanical efficiency. This shows that it is possible to estimate within a 10% accuracy the volumetric efficiency of a particular design without recurring to slow CFD models. Efforts in the refinement in the estimation models for the mechanical efficiency are still required, as well as the incorporation of other fast simulation methodologies that could enrich the design tool.

Funding This work was funded by the Basque Government/Eusko Jarlitza Grant Number ZL-2020/00190.

Declarations

Conflict of interest The authors declare no Conflict of interest in this work.

References

1. Hill, M.: Kinematics of Gerotors. Reilly (1927)
2. Hussain, T., Kumar, M.U., Sarangi, N., Sivaramakrishna, M.: A study on effect of operating conditions on gerotor pump performance. Def. Sci. J. **72**(2), 146 (2022)
3. Mancò, S., Nervegna, N., Rundo, M., Margaria, M.: Miniature gerotor pump prototype for automotive applications. In: Proceedings of the 3rd IFK International Fluid Power Conference, Aachen, Germany, pp. 5–6 (2002)
4. Gamez-Montero, P.J., Codina, E., Castilla, R.: A review of gerotor technology in hydraulic machines. Energies **12**(12), 2423 (2019)
5. Ruvalcaba, M. A., Hu, X.: Gerotor fuel pump performance and leakage study. In: ASME International Mechanical Engineering Congress and Exposition, vol. **54921**, pp. 807–815 (2011)
6. Segonds, F., Cohen, G., Véron, P., Peyceré, J.: PLM and early stages collaboration in interactive design, a case study in the glass industry. Int. J. Interact. Des. Manuf. (IJIDeM) **10**, 95–104 (2016)
7. Beitz, W., Pahl, G., Grote, K.: Engineering design: a systematic approach. MRS Bull. **21**, 71 (1996)
8. Gannesh, V.T., Sivakumar, R., Sakthivel, G.: Fixed displacement gerotor oil pump (FDOP): a survey. Int. J. Ambient Energy **43**(1), 2328–2338 (2022)
9. Hsieh, C.-F.: Flow characteristics of gerotor pumps with novel variable clearance designs. J. Fluids Eng. **137**(4), 041107 (2015)
10. Castilla, R., Gamez-Montero, P.J., Raush, G., Codina, E.: Method for fluid flow simulation of a gerotor pump using OpenFOAM. J. Fluids Eng. **139**(11), 111101 (2017)
11. Lee, M.-C., Kwak, H.-S., Seong, H., Kim, C.: A study on theoretical flowrate of gerotor pump using chamber areas. Int. J. Precis. Eng. Manuf. **19**(9), 1385–1392 (2018)
12. Ivanović, L., Josifović, D., Blagojević, M., Stojanović, B., Ilić, A.: Determination of gerotor pump theoretical flow. In: 1st International Scientific Conference, Conference on Mechanical, Engineering Technologies and Applications, pp. 243–250 (2012)
13. Gamez-Montero, P.J., Codina, E.: Flow characteristics of a trochoidal-gear pump using bond graphs and experimental measurement. Part 2. Proc. Inst. Mech. Eng. Part I J. Syst. Control Eng. **221**(3), 347–363 (2007)

14. Lingeswaramurthy, P., Jayabhaskar, J., Elayaraja, R., Suresh Kumar, J.: Development of analytical model for design of gerotor oil pump and experimental validation. SAE Int. J. Engines **4**(1), 441–449 (2011)
15. Liu, H., Lee, J.-C., Yoon, A., Innotek, L.G., Kim, S.-T., Innotek, L.G.: Profile design and numerical calculation of instantaneous flow rate of a gerotor pump. J. Appl. Math. Phys. **3**(01), 92 (2015)
16. Harrison, J., Aihara, R., Eisele, F.: Modeling gerotor oil pumps in 1D to predict performance with known operating clearances. SAE Int. J. Engines **9**(3), 1839–1846 (2016)
17. Inaguma, Y.: Friction torque characteristics of an internal gear pump. Proc. Inst. Mech. Eng. C J. Mech. Eng. Sci. **225**(6), 1523–1534 (2011)
18. Inaguma, Y.: Oil temperature influence on friction torque characteristics in hydraulic pumps. Proc. Inst. Mech. Eng. C J. Mech. Eng. Sci. **226**(9), 2267–2280 (2012)
19. Ivanović, L.: Reduction of the maximum contact stresses by changing geometric parameters of the trochoidal gearing teeth profile. Meccanica **51**(9), 2243–2257 (2016)
20. Kwak, H.S., Li, S.H., Kim, C.: Optimal design of the gerotor (2-ellipses) for reducing maximum contact stress. J. Mech. Sci. Technol. **30**(12), 5595–5603 (2016)
21. Ivanović, L., Rakić, B., Stojanović, B., Matejić, M.: Comparative analysis of analytical and numerical calculations of contact stresses at rotational elements of gerotor pumps. Appl. Eng. Lett **1**(1), 1–7 (2016)
22. Ivanovic, L., Devedzic, G., Miric, N., Cukovic, S.: Analysis of forces and moments in gerotor pumps. Proc. Inst. Mech. Eng. C J. Mech. Eng. Sci. **224**(10), 2257–2269 (2010)
23. Ping, X., Yang, F., Zhang, H., Zhang, J., Zhang, W., Song, G.: Introducing machine learning and hybrid algorithm for prediction and optimization of multistage centrifugal pump in an orc system. Energy **222**, 120007 (2021)
24. Bustillo, A., Urbikain, G., Perez, J.M., Pereira, O.M., de Lacalle, L.N.L.: Smart optimization of a friction-drilling process based on boosting ensembles. J. Manuf. Syst. **48**, 108–121 (2018)
25. Gamez-Montero, P.J., Castilla, R., Mujal, R., Khamashta, M., Codina, E.: Gerolab package system: innovative tool to design a trochoidal-gear pump (2009)
26. Nee, A.Y.C., Ong, S.K.: Special issue on digital twins in industry (2021)
27. Yang, B., Yang, S., Lv, Z., Wang, F., Olofsson, T.: Application of digital twins and metaverse in the field of fluid machinery pumps and fans: a review. Sensors **22**(23), 9294 (2022)
28. Morley, F.: On adjustable cycloidal and trochoidal curves. Am. J. Math. **16**(2), 188–204 (1894)
29. Javier, P., Montero, G.: Fluid-Dynamics Characterization of an Internal Gear Oleohydraulic Pump with Trochoidal Profiles. Ph.D. Thesis, Universitat Politècnica de Catalunya (2004)
30. White, F.M.: Fluid mechanics. The McGraw Hill Companies (2008)
31. Altare, G., Rundo, M.: Computational fluid dynamics analysis of gerotor lubricating pumps at high-speed: geometric features influencing the filling capability. J. Fluids Eng. **138**(11), 111101 (2016)